NJC

PAPER

View Article Online
View Journal | View Issue

Published on 13 March 2019. Downloaded by National Synchrotron Radiation Research on 1/9/2020 4:40:19 AM.

Check for updates

Cite this: *New J. Chem.*, 2019, **43**, 5623

Hydrogenation of dioctyl phthalate over a Rh-supported Al modified mesocellular foam catalyst

Avinash B. Lende, Saurav Bhattacharjee, Wei-Yuan Lu and Chung-Sung Tan *

Received 23rd January 2019,
Accepted 13th March 2019

DOI: 10.1039/c9nj00404a

rsc.li/njc

A new catalyst was developed for selective hydrogenation of dioctyl phthalate (DOP) to produce the environmentally friendly plasticizer di(2-ethylhexyl)hexahydrophthalate (DEHHP) by incorporating rhodium *via* chemical fluid deposition into an aluminum-modified mesocellular foam (MCF). The Al-modified MCF containing a Si/Al molar ratio of 5 and 1 wt% Rh achieved 100% conversion of DOP to DEHHP with no side products at 80 °C and 68 atm H_2 pressure in one hour reaction time. On the other hand, a 1 wt% Rh/MCF catalyst without any surface modification with Al yielded only 29% conversion. The interaction of Rh with the support became stronger when Al was incorporated onto the MCF support. An effective control of the acidity provided by Al by closely monitoring the Si/Al ratio was key in improving the catalytic activity of the Rh/Al-MCF catalysts.

Introduction

Dioctyl phthalate (DOP) has been widely used in plastic industries to enhance the flexibility and durability of products, especially with polyvinyl chloride (PVC) in food packaging, toys and medical devices. The global market for plasticizers has increased from 5.6 to 8.4 million metric tons within the last decade.[1] The total growth rate was estimated to increase by 6.35% annually, with 87% of this growth being phthalate plasticizers. Phthalates have been identified as one of the main chemical agents that could cause cancer, obesity and reproductive problems.[1] Human beings could experience anti-steroidal activity after the interaction of phthalates with human keto-steroids such as androgen and glucocorticoid. Phthalate and its derivatives bind with proteins and could affect human serum albumin.[2] Because of the unfavorable and toxic nature of phthalates, it remains a huge challenge to make phthalate-free plasticizers for various applications.

Several researchers have investigated the complete hydrogenation of DOP with different types of supported metal catalysts.[3–7] One method is to hydrogenate the benzene ring of phthalate compounds. In the phthalate compound, the benzene ring is connected to the electron withdrawing ester groups making it a challenge to selectively hydrogenate the benzene ring.[4] Obtaining phthalate-free plasticizers requires noble metal catalysts. Various researchers have used supported Rh, Pt and Pd catalysts for the hydrogenation of phthalates.[8–11] The choice of support plays an important role in improving the efficiency of the noble-metal-based catalysts.[12,13] The properties of supports significantly affect the catalytic performances of the supported metals. The reducibility and dispersion of supported metals depend on the interactions between the support and the supported metals. In addition, the surface acidic and basic properties also play important roles in determining the catalytic activity.[14,15]

Meso-porous materials are a perfect candidate as a catalyst support due to their tunable pore size, structure and internal connectivity. Different types of meso-porous materials, such as MCM-41 and SBA-15, have been employed as supports.[16,17] However, both MCM-41 and SBA-15 have typical two dimensional (2D) hexagonal meso-structures. In addition, the pore sizes of MCM-41 and SBA-15 are relatively small, giving rise to a large diffusion resistance. Using three dimensional (3D) meso-structures as supports may reduce diffusion resistance and increase catalyst dispersion in the support. Silica materials such as mesocellular foam (MCF) display especially large pore sizes, high surface areas, large pore volumes and uniform size ranges.[18–23] The ability to tune their textural properties makes MCFs a promising candidate as a catalytic support. However, compared with microporous zeolites, MCFs have substantially weaker acidity because of their electronically neutral Si frameworks, which limit their applications in acid-catalyzed reactions.

The incorporation of transition metals such as Al, Ti, and Zr onto Si-based supports is used to improve the acidity of silica materials and thus increases catalytic performance in acid-catalyzed reactions. Al-Modified supports have been reported to enhance the efficiency of hydrogenation reactions.[24,25] Kustrowski *et al.* reported that transition metals doped on MCF were the best support for hydrogenation of aromatic compounds when compared to the smaller pore sized and hydrothermally unstable Al-MCM-48 or Al-SBA-15.[26] Debecker *et al.* also reported a better performance of macro–mesocellular silica–alumina foam synthesized *via* the sol–gel method for the dehydration of bioethanol to ethane.[27]

Department of Chemical Engineering, National Tsing Hua University, Hsinchu, Taiwan, 30013, Republic of China. E-mail: cstan@mx.nthu.edu.tw

Published on 13 March 2019. Downloaded by National Synchrotron Radiation Research on 1/9/2020 4:40:19 AM.

In recent years, chemical fluid deposition (CFD) has received considerable attention for depositing metals onto mesoporous supports. It has been used to generate a wide variety of mono or multi-metallic catalysts. Because supercritical CO_2 possesses several unique properties including negligible surface tension, liquid-like density, gas-like viscosity, dissolving power towards organic compounds, and high mass transfer rate as well as being non-toxic and abundant, it has been widely used as the solvent in CFD. Compared to the conventional methods, agglomeration of nanoparticles on the surface of porous supports was reduced by using CFD, leading to a better dispersion of active metal sites and consequently affecting the catalyst activity.[28–30]

In this study, a Rh_x/Al_y-MCF catalyst (where x denotes the wt% loading of Rh and y denotes the Si/Al molar ratio) synthesized by CFD was used for 100% selective, solvent-free hydrogenation of DOP to the phthalate-free plasticizer di(2-ethylhexyl)hexahydrophthalate (DEHHP). The catalysts were characterized using various analytical tools, and several reaction variables were studied to obtain the most favorable reaction conditions. The effect of the amount of Al incorporated onto MCF on catalytic performance was investigated as well.

Experimental section

Chemicals

Triblock copolymer P123 (PEO_{20}–PPO_{70}–PEO_{20}; PEO: polyethylene oxide; PPO: polypropylene oxide) with a MW $\sim$ 5800 g mol^{-1} and a purity > 98% and chloroform-*d* ($CDCl_3$, purity > 99.8%) were purchased from Sigma Aldrich. 1,3,5-Trimethylbenzene (TMB, purity > 99%), tetraethyl orthosilicate (TEOS, purity > 98%), ammonium fluoride (NH_4F, purity > 99%), aluminum chloride ($AlCl_3$, purity > 99) and dioctyl phthalate (DOP, purity 99%) were purchased from Alfa Aesar. Rhodium(III) acetylacetonate $Rh(acac)_3$ having a purity > 99% was purchased from Acros Organics. Tetrahydrofuran (THF, purity > 98%) and ethanol (EtOH, purity > 99%) were purchased from Choneye Pure Chemicals. Hydrochloric acid (HCl, purity > 97%) was purchased from Honeywell. H_2 was purchased from Boclh Industrial Gases Co., Ltd (TW). All chemicals and gases were used as received without any further purification.

Synthesis of MCF

MCF was synthesized by modifying a previously reported synthesis method.[31,32] The triblock copolymer P123 (4 g) was dissolved in 75 mL of an aqueous HCl solution (1.6 M) at room temperature with TMB (4 g) as the organic swelling agent. The solution was kept at a temperature of 40 °C and stirred for 2 h. Then, TEOS (9.2 g) was added separately and again stirred for 0.5 h. The mixture was transferred to an autoclave and aged at 40 °C for 24 h. Then, NH_4F (45 mg) was added as an inorganic mineralizing agent and the mixture was further aged at 140 °C for 24 h. The precipitated material was isolated by filtering and washing, and dried at 80 °C for 2 h. Finally, the sample was calcined in air at 550 °C for 6 h to remove the template material.

Synthesis of Al-MCFs

To synthesize Al_y-MCFs, $AlCl_3$ was used as the aluminum source and EtOH was used as the solvent. The procedure for the post-synthesis of Al-MCFs followed the method reported by Lim *et al.* 2 g of MCF was mixed with 100 mL of EtOH at room temperature and the mixture was stirred for 15 min.[31] Then, a fixed amount of $AlCl_3$ was added to obtain the desired ratio of Si/Al. The obtained solution was stirred for 5 h, and then filtered and washed with EtOH, and finally dried at 80 °C for 2 h. The amount of $AlCl_3$ used in the post-synthesis method resulted in the Si/Al molar ratios of 5, 10 and 20.

Synthesis of Rh_x/Al_y-MCFs

The Rh_x/Al_y-MCFs were synthesized using the CFD method. For a typical synthesis of Rh_1/Al_5-MCF, 0.011 g of $Rh(acac)_3$ was added to 30 mL of THF containing 0.3 g of Al_5-MCF. The mixture was ultrasonicated for 2 h to speed up the impregnation. THF was then evaporated using a rotary evaporator and the collected powders were transferred into a high-pressure stainless steel reactor to redisperse the metal precursors into the pores of Al_y-MCFs with pressurized CO_2 at 40 °C and 170 atm for 2 h. Afterward, the reactor was depressurized to ambient pressure and cooled down to a temperature of 5 °C. The treated catalysts were calcinated at 550 °C for 4 h followed by a reduction by H_2 at 400 °C for 4 h.[25,28,29]

Catalyst characterization

The specific surface area of the synthesized catalysts was measured using the Brunauer–Emmett–Teller (BET) method, while pore diameters and windows were measured using the BJH adsorption and desorption methods, respectively (Micromeritics, 2060). ^{27}Al-NMR (Bruker, Ultrashield 400) was used for the solid NMR analysis. The wide-angle X-ray diffraction data were obtained with Cu-Kα radiation of 40 kV and 20 mA, a scan rate of 5° min^{-1} and a 2θ range from 10–70° (Rigaku, 9407F701n). Low-angle XRD was conducted with an X-ray detector having a pixel size of 0.158 mm (MAR, BL23A) with the beam center at (x: 512.1, y: 581.0) having 12 keV photon energy. SEM images were obtained by using a UHR cold-emission scanning electron microscope (JEOL, JSM-7000F). EDX was conducted on an energy dispersive X-ray instrument (Oxford, 42221-5450-TV3-4739). For recording TEM images, a TEM (JOEL, JEM-2100) HT transmission electron microscope operating at 200 kV was used. A drop of EtOH containing suspended catalyst was placed on a 200 mesh carbon-coated copper grid and allowed to dry overnight before use for TEM characterization. XPS was undertaken using a high-resolution X-ray photoelectron spectrometer (ULVAC-PHI XPS, PHI Quantera) with a 180° spherical capacitor analyzer and a +32 channel detector. NH_3-TPD and H_2-TPR (Micromeritics, ASAP 2920) were carried out using a quartz tube flow reactor equipped with a TCD detector.

Catalytic hydrogenation

The solvent-free hydrogenation of DOP was carried out in a semi-continuous mode in a 180 mL stainless steel reactor equipped

 This journal is © The Royal Society of Chemistry and the Centre National de la Recherche Scientifique 2019

Published on 13 March 2019. Downloaded by National Synchrotron Radiation Research on 1/9/2020 4:40:19 AM.

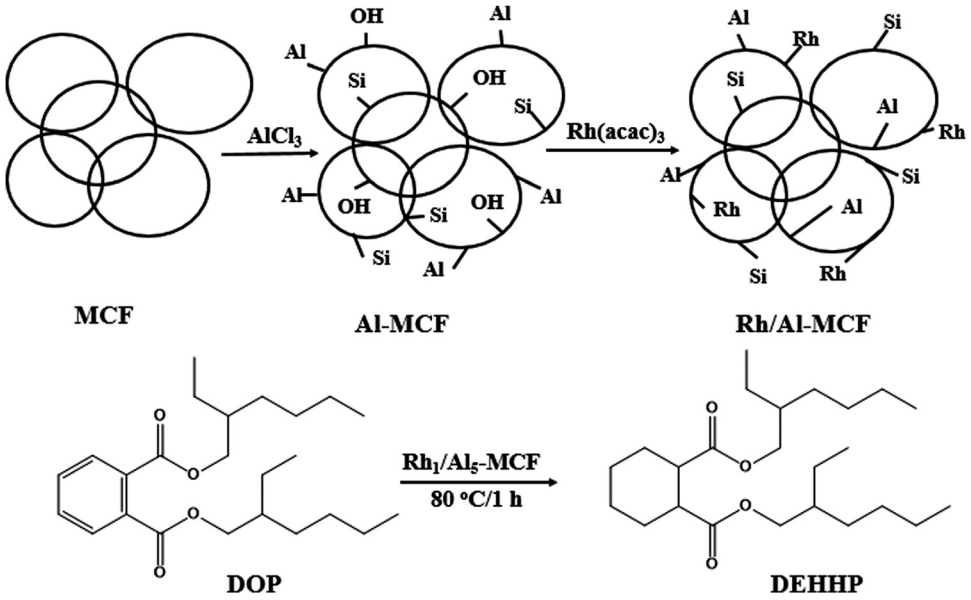

Fig. 1 The schematic of the synthesis of the Rh-supported Al-MCF catalyst and the hydrogenation of DOP to DEHHP.

with a magnetic stirrer (Parr Instruments, 57308). The reactor was connected to a H_2 cylinder to ensure a continuous supply of H_2. In a typical experiment, the desired amounts of DOP and catalyst were charged into the reactor. The reactor was sealed and purged 2–3 times with pressurized H_2 gas to remove the air. The reactor was then heated to the desired reaction temperature to allow the reaction to start. After the completion of the reaction, the solid catalyst was collected from the solution by centrifugation. The conversion was determined by using ^{1}H-NMR with $CDCl_3$ as the solvent. The reaction conditions were set as a stirring speed of 1000 rpm, a reaction time of 1 h, a mass of catalyst of 25 mg and a mass of reactant of 5 g for all the experimental runs. To ensure reproducibility of the experimental results, the experiments were reperformed by maintaining the same reaction conditions. The data were observed to be reproducible within a 2% variation. The conversion was calculated from ^{1}H-NMR spectra using the single proton peak area for the reactant and product. The synthesis of the rhodium-supported Al-MCF catalyst and the hydrogenation of DOP are shown in Fig. 1.

Results and discussion

Physical properties of the supports and catalysts

The specific surface areas of SBA-15, virgin MCF and various modified catalysts were determined using the BET area analyzer method. The total pore volume (V_p, $cm^3\ g^{-1}$), pore diameter (D_p, nm) and window size (D_w, nm) of SBA-15, MCF, Al_{10}-MCF, Al_5-MCF, Rh_1/MCF, Rh_1/Al_{10}-MCF and Rh_1/Al_5-MCF are summarized in Table 1. It can be seen that in comparison to SBA-15, MCF had a smaller surface area with much larger pore diameters, due to a phase change brought about from the ordered hexagonal symmetry of SBA-15 to the inter-connected cage-like structure of MCF on addition of a hydrophobic swelling agent. All the fresh

Table 1 Textural properties of the synthesized supports and catalysts

Material	S_{BET} ($m^2\ g^{-1}$)	V_p ($cm^3\ g^{-1}$)	D_p (nm)	D_w (nm)
SBA-15	695	2.1	5.3	—
MCF	510	4.4	30.5	12.5
Al_{10}-MCF	447	3.1	24.1	12.1
Al_5-MCF	392	2.5	22.7	11.9
Rh_1/MCF	337	3.2	29.2	11.7
Rh_1/Al_{10}-MCF	321	2.1	21.3	11.9
Rh_1/Al_5-MCF	315	1.7	21.3	11.7

and Rh impregnated Al_y-MCFs exhibited narrow distributions of mesopores with large pore diameters (~30 nm) connected to each other *via* windows (~12 nm). The BET and BJH analyses of the Rh impregnated Al_y-MCF catalysts showed that S_{BET} and D_W of the catalysts were not changed significantly after catalyst synthesis as compared to the Al_y-MCF supports, indicating that the impregnation of Rh did not block the pore openings of the Al_y-MCF supports. The morphologies of the synthesized MCF and Al_5-MCF supports and the Rh_1/MCF and Rh_1/Al_5-MCF catalysts are shown in Fig. 2. There were no significant changes in the morphology of MCF after the incorporation of Al. The SEM-EDX images ofAl_5-MCF shown in Fig. 3 indicate a uniform dispersion of Al on MCF.

The TEM images of SBA-15 and MCF (Fig. 4a and b) clearly show how the ordered hexagonal morphology of SBA-15 was changed to a disordered inter-connected cage-like structure of MCF on the addition of a hydrophobic swelling agent. Modification of MCF with Al also showed no significant effect on the morphology and the structure of MCF (Fig. 4d and e). This observation was consistent with the observed SEM results and the reported observation for a MCF based catalyst.[25] Fig. 4f and g revealed that post catalyst synthesis, the Rh nanoparticles were located primarily inside the pores of the MCF and the Al_y-MCF supports. The average particle size of the Rh nanoparticles

Published on 13 March 2019. Downloaded by National Synchrotron Radiation Research on 1/9/2020 4:40:19 AM.

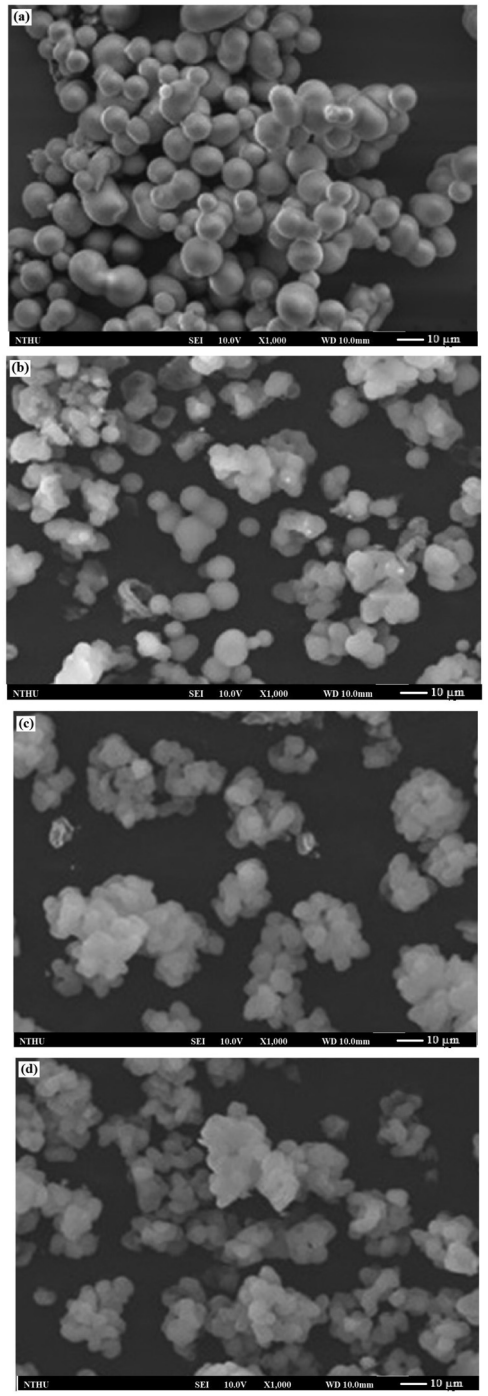

Fig. 2 SEM images of the synthesized Al_y-MCF materials and catalysts with different Si/Al ratios: (a) MCF, (b) Rh_1/MCF, (c) Al_5-MCF and (d) Rh_1/Al_5-MCF.

measured using ImageJ software (~6 nm) was found to be smaller than the pore openings of MCF and Al_y-MCF (~12 nm). This suggested that the nanoparticle formation was controlled by the pore openings of the supports. Since all the MCF supported catalysts studied in this work possessed an average Rh particle size of 6 nm, the effect of Rh particle size on the reaction of DOP to DEHHP was not examined in this study.

Fig. 5(a) and (b) show the wide-angle and low-angle XRD patterns of the synthesized Rh_1/MCF and Rh_1/Al_y-MCF catalyst materials with different Si/Al ratios, respectively. No crystalline diffraction peaks were observed for all samples, indicating that the Al and Rh species were either well-dispersed on the silica supports or the crystallite species were too small to be detected by wide-angle XRD.[33] This observation also verified an even dispersion of metal in the catalyst when the CFD method was used for catalyst preparation. A very low Rh loading of 1 wt% might be another reason for not observing any Rh diffraction peaks in the wide-angle XRD results. From Fig. 5(b), it can be seen that the low-angle XRD patterns of the synthesized supports and the catalysts exhibited almost the same peaks, indicating that the structural integrity of the parent support material was retained on incorporation of Rh nanoparticles into the support by CFD. This was attributed to the low surface tension of $scCO_2$.

Chemical properties of the supports and the catalysts

The ^{27}Al-NMR spectra of Al_y-MCF materials with varied Si/Al ratios and the Rh_1/Al_5-MCF catalyst were obtained to study the state of Al in the catalyst supports. Fig. 6 shows three intense peaks at 0, 33 and 54 ppm at which an Al atom was covalently bonded to eight, five and four Si atoms through oxygen bridges, respectively. The formation of Al–O–Si bridges in the tetrahedral geometry yielded stronger acid sites or Brønsted acid sites as compared to those in the octahedral and pentahedral geometries, which revealed weak acid sites or Lewis acid sites of the catalysts. The detection of tetrahedrally coordinated Al^{3+} cations confirmed that the Al species had been successfully incorporated into the MCF framework. The modified supports exhibited tetrahedral geometry at high Si/Al ratios and moved towards pentahedral and octahedral geometries as the Si/Al ratio decreased due to the formation of Al–O–H bridges.[25]

The strength of the acid sites was measured by the desorption temperature of NH_3. Based on the desorption temperatures, the peaks were classified as physically adsorbed NH_3 (100–250 °C), weak acid sites (250–400 °C) and strong acid sites ($T > 400$ °C). The peaks were treated mathematically using a Gaussian function. As can be seen in Fig. 7, all the catalysts showed weak and strong acid sites. The concentrations of weak and strong acid sites, and total strength of the catalysts, expressed as mmoL of desorbed NH_3 g^{-1} catalyst, are given in Table 2. The results showed an increase in acid sites from strong to weak, as the Si/Al ratio decreased. Compared to the Rh_1/MCF catalyst, the Rh_1/Al_5-MCF catalyst yielded an increase of nearly 32% in weak acid sites. Huirache *et al.* reported that the strength of acid sites was responsible for the hydrogenation of aromatic compounds.[34] The results discussed later in this study confirmed the fact that it was the weak acid sites of the catalyst that strongly influenced the conversion rate of the reaction. Acid–base titration can be used as an additional tool to measure the acidic and basic sites of catalysts[35] and it is being considered for further studies involving the use of modified silica materials as catalyst supports.

The observed spectra are shown in Fig. 8. The binding energies in the 304.0–311.9 eV and 312.0–318.0 eV regions

 This journal is © The Royal Society of Chemistry and the Centre National de la Recherche Scientifique 2019

Published on 13 March 2019. Downloaded by National Synchrotron Radiation Research on 1/9/2020 4:40:19 AM.

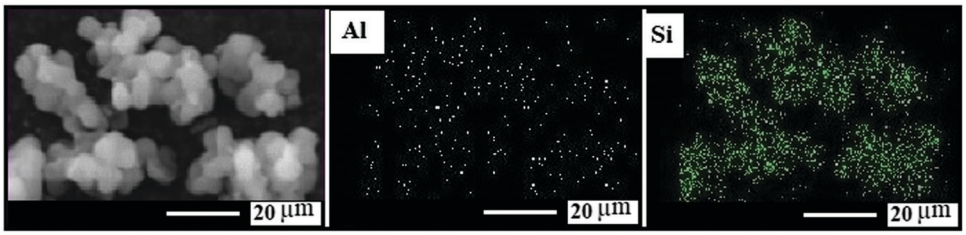

Fig. 3 SEM-EDX images of the synthesized Al_5-MCF material.

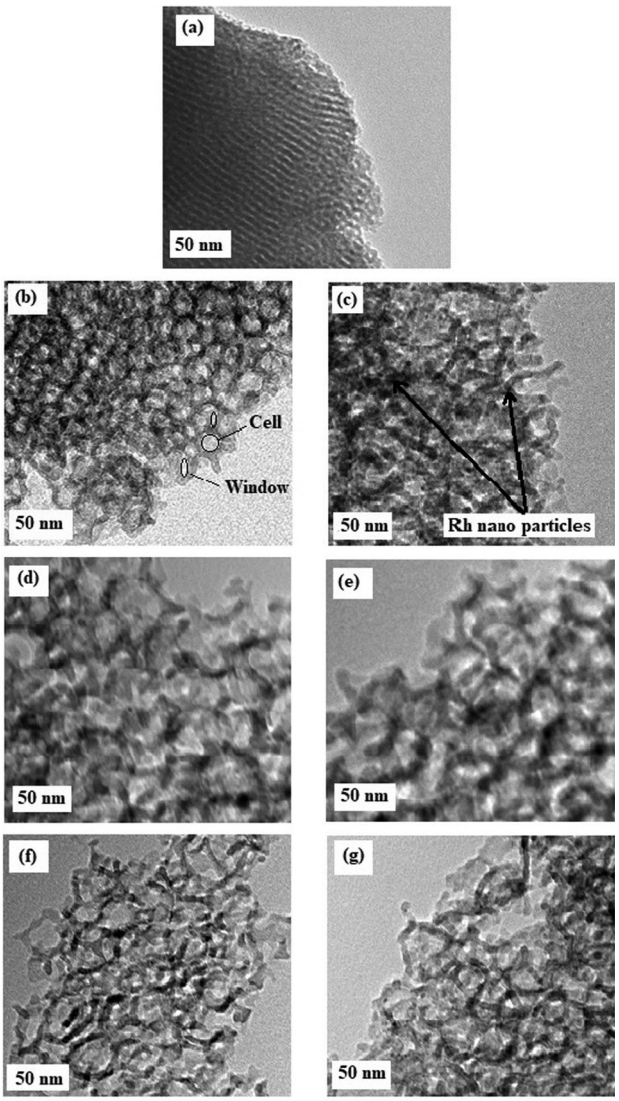

Fig. 4 TEM images of the synthesized supports and catalysts: (a) SBA-15, (b) MCF, (c) Rh_1/MCF, (d) Al_{10}-MCF, (e) Al_5-MCF (f) Rh_1/Al_{10}-MCF (g) Rh_1/Al_5-MCF.

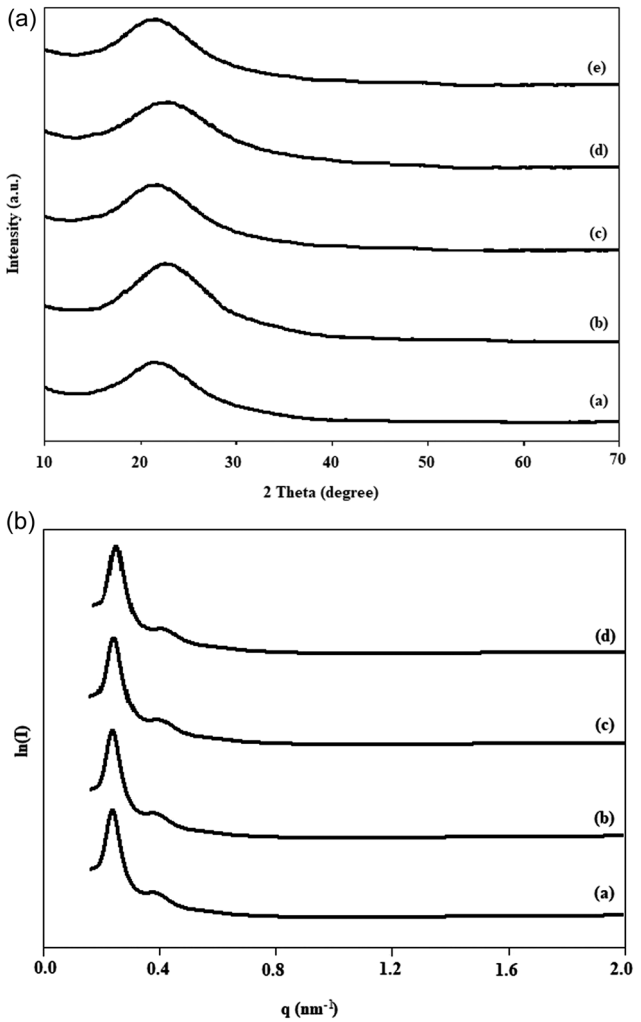

Fig. 5 (a) Wide-angle XRD patterns of the synthesized supports and catalysts: (a) MCF, (b) Al_5-MCF, (c) Rh_1/MCF, (d) Rh_1/Al_5-MCF and (e) Rh_1/Al_{10}-MCF. (b) Low-angle XRD patterns of the synthesized supports and catalysts: (a) MCF, (b) Al_5-MCF, (c) Rh_1/MCF and (d) Rh_1/Al_5-MCF.

could be attributed to Rh $3d_{5/2}$ and Rh $3d_{3/2}$, respectively. All the Rh (3d) spectra were fitted by using two sets of doublets that correspond to the metallic Rh^0 and oxidized Rh^{3+} chemical environments. Rh $3d_{5/2}$ binding energy regions have been reported to occur at 307.2 (±0.2) eV for Rh^0 and 308.7 (±0.3) eV for Rh^{3+}. The relative abundance of the surface Rh^0 and Rh^{3+} species of each catalyst was calculated by considering the de-convoluted Rh $3d_{5/2}$ signal and the atomic% of the degrees of oxidation of Rh, as shown in Table 3. The results indicated that the Rh_1 particles supported on MCF possessed Rh^{3+} and Rh^0 species in the presence of a transition metal (Al). The Rh^{3+} atomic ratio was higher at a Si/Al ratio of 20 when compared to 10 and 5, due to overcrowding of Al species at the lower Si/Al

Published on 13 March 2019. Downloaded by National Synchrotron Radiation Research on 1/9/2020 4:40:19 AM.

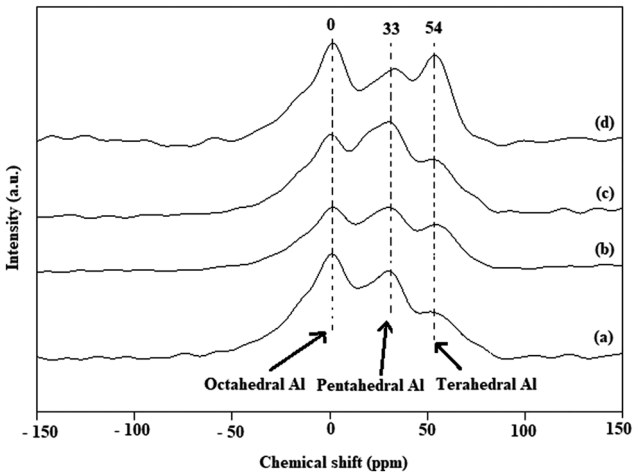

Fig. 6 ^{27}Al-NMR spectra of the synthesized supports and catalyst: (a) Al_5-MCF, (b) Al_{10}-MCF, (c) Al_{20}-MCF and (d) Rh_1/Al_5-MCF.

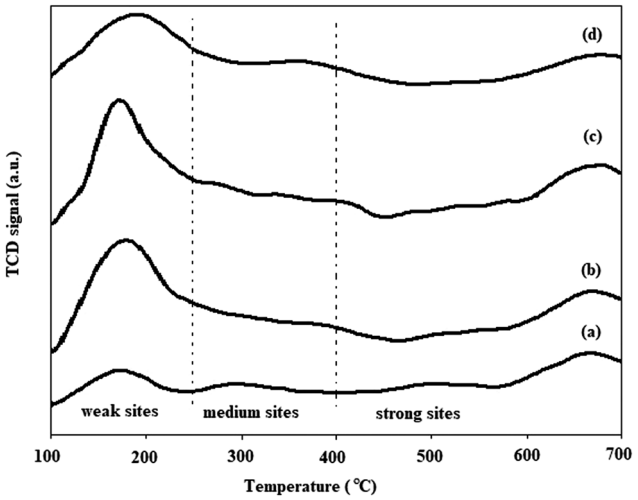

Fig. 7 NH_3-TPD profiles of the synthesized catalysts: (a) Rh_1/MCF, (b) Rh_1/Al_{20}-MCF, (c) Rh_1/Al_{10}-MCF and (d) Rh_1/Al_5-MCF.

Table 2 Acidic properties of the synthesized catalysts as determined by NH_3-TPD

Catalyst	Number of acid sites (mmol NH_3 g_{cat}^{-1})		Strength of acid sites
	Weak	Strong	
Rh_1/MCF	0.08	0.13	0.21
Rh_1/Al_{20}-MCF	0.18	0.01	0.19
Rh_1/Al_{10}-MCF	0.23	0.03	0.26
Rh_1/Al_5-MCF	0.25	0.05	0.30

ratios affecting the distribution of Rh species in the catalyst. For the Rh_1/MCF catalyst with no Al modification, only Rh^{3+} species were observed. Also, the Al-modified catalysts possessed a higher binding energy for Rh $3d_{5/2}$ when compared to the Rh_1/MCF catalyst, highlighting a sturdy interaction that may arise between the Rh nanoparticles and the surface OH groups of Al in Al_y-MCF. This theory can be backed up by the data shown in Table 3, where, for the Al_y-MCF supported catalysts, the ratio of Rh^{3+}/Rh^0 species reduced significantly as the Si/Al ratio went down from 20 to 10, signifying a correlation between acidity and the formation of Rh^{3+} or Rh^0. However, at a Si/Al ratio of 5, the Rh^{3+}/Rh^0 ratio was the same as at a Si/Al ratio of 10, indicating that the effect of acidity on the formation of different oxidation states of Rh species might remain unchanged after a certain value.

The H_2-TPR results revealed several oxidation states of Rh in Rh_1/Al_y-MCF. The interaction among metal, metal oxide and support was directly dependent on increasing reduction temperature. The H_2-TPR thermograms for the Rh_1/MCF and Rh_1/Al_y-MCF catalysts are shown in Fig. 9. For the Rh_1/MCF catalyst, a small peak at 60 °C arose, possibly due to the reduction of a weak oxidation layer on the metal that formed when the catalyst contacted with air. Other peaks at 250 °C and 371 °C could be attributed to the bulk reduction of Rh, implying strong interaction with the support, as can be seen in Fig. 9(a). Fig. 9(b) shows that upon introduction of Al, for the Rh_1/Al_{20}-MCF catalyst, there existed only one H_2 consumption peak at 155 °C, attributed to the surface reduction of RhO_x.

As the Al content was increased further, the H_2 consumption signal for the surface reduction of RhO_x started to increase (163 °C) and became sharper, indicating stronger interaction between the metal oxide and the support, Rh_1/Al_{10}-MCF, see Fig. 9(c). A bulk reduction peak at 388 °C once again reappeared for the Rh_1/Al_{10}-MCF catalyst. For the Rh_1/Al_5-MCF catalyst, only bulk reduction peaks appeared (363 °C), representing a maximum interaction between metal and support at a Si/Al ratio of 5 in Fig. 9(d).

Effect of porous catalyst supports

The type of catalyst support was found to have a strong influence on catalyst performance. A meso-porous silica support having a high surface area and uniform pore structure was considered to be more desirable and attractive for catalytic reactions.[36,37] The BET surface areas of SBA-15 and MCF were 695 and 510 m^2 g^{-1}, respectively. The total pore volumes were 2.1 and 4.48 cm^3 g^{-1} with an average pore diameter of 5.3 and 12.5 nm, respectively (Table 1). It was found that the addition of a hydrophobic swelling agent during the synthesis of SBA-15 induced a phase conversion from the well-ordered hexagonal symmetry of SBA-15 to an interconnected cage-like structure of MCF. This 3-dimensional cage-like structure was ideally suited to act as a catalyst support for the hydrogenation of bulky aromatic hydrocarbons by reducing internal diffusion resistance. 29% conversion was observed using the Rh_1/MCF catalyst for the hydrogenation of DOP to DEHHP at 80 °C and 68 atm H_2 pressure, as compared to a 3.5% conversion obtained using the Rh_1/SBA-15 catalyst. The molecular sizes of the reactant (DOP) and the desired product (DEHHP) calculated using ChemDraw 3D pro V12 were 1.0 and 1.3 nm, respectively. Therefore, although diffusion resistance definitely played some if not a detrimental role in determining the conversion of DOP to DEHHP, it was also reasoned that the 3-dimensional cage-like structure of MCF played a crucial role in increasing the conversion of DOP using a MCF supported

 This journal is © The Royal Society of Chemistry and the Centre National de la Recherche Scientifique 2019

Published on 13 March 2019. Downloaded by National Synchrotron Radiation Research on 1/9/2020 4:40:19 AM.

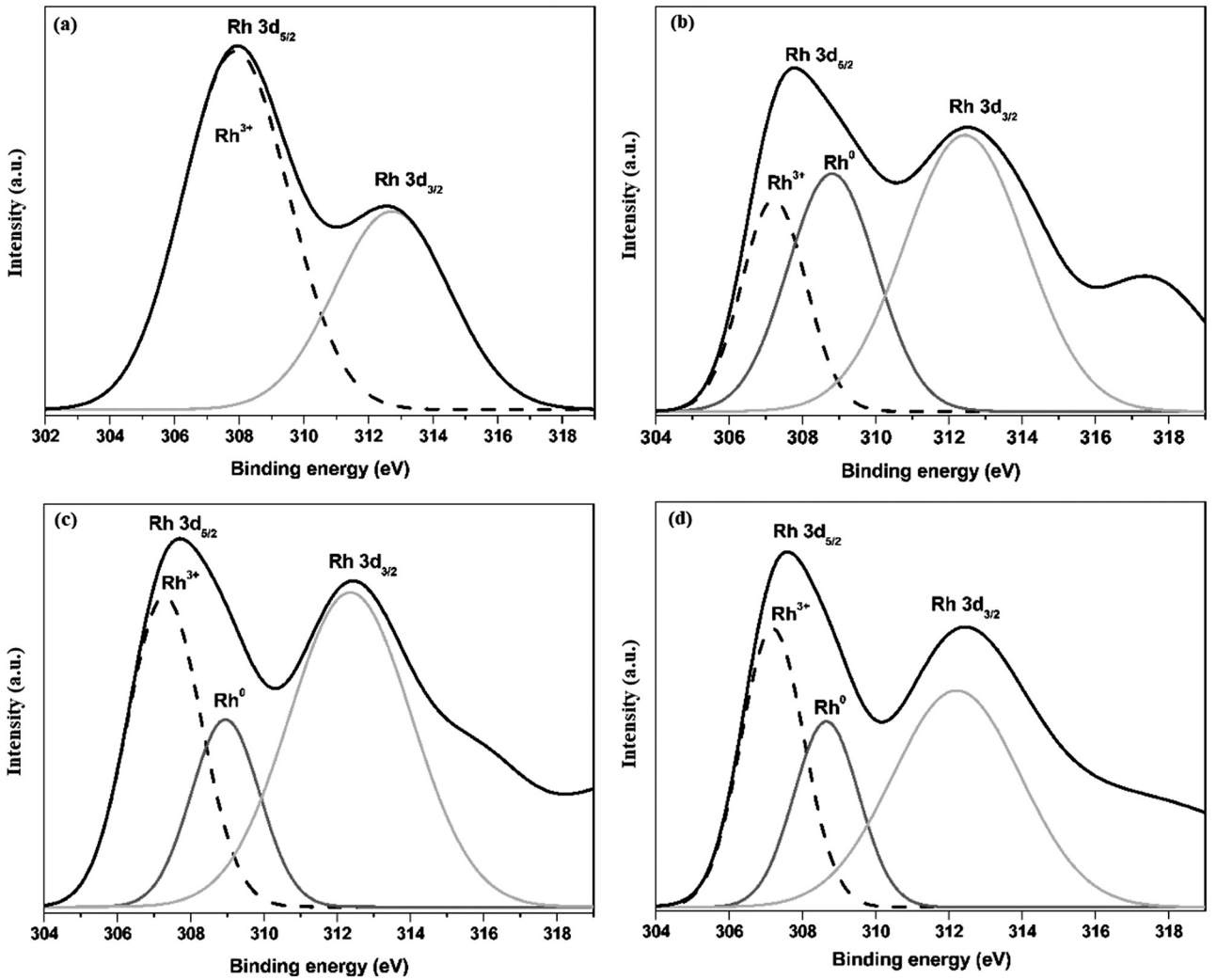

Fig. 8 XPS spectra of the synthesized catalysts in the Rh (3d) core level region: (a) Rh_1/MCF, (b) Rh_1/Al_{20}-MCF, (c) Rh_1/Al_{10}-MCF and (d) Rh_1/Al_5-MCF.

Table 3 XPS results of the curve fitting of the Rh $3d_{5/2}$ peak for the synthesized catalysts

Catalyst	Rh^{3+} (atom%)	Rh^{3+} BE (eV)	Rh^0 (atom%)	Rh^0 BE (eV)	FWHM[a] Rh $3d_{5/2}$ (eV)	Rh^{3+}/Rh^0
Rh_1/MCF	100	308.1	—	—	3.8	—
Rh_1/Al_{20}-MCF	92.4	308.7	7.6	307.1	2.7	12.1
Rh_1/Al_{10}-MCF	79.7	308.9	20.3	307.2	3.1	3.9
Rh_1/Al_5-MCF	79.7	308.6	20.3	307.1	2.7	3.9

[a] Full width at half maximum.

catalyst compared to an SBA-15 supported one. The 3-dimensional structure of MCF helped more H_2 species to access the active metal sites from all sides, leading to increased H_2 spillover[38] and subsequently an enhancement in the reaction rate and an increase in the conversion of DOP to DEHHP. Thus, MCF was believed to be superior to SBA-15 and was used as the support for further studies.

Effect of surface modification of MCF with Al on catalytic performance

It can be seen from Table 4 that as the Si/Al ratio decreased from 20 to 10 and then to 5, the conversion of DOP to DEHHP increased from 45 to 62% and finally to 100% at 80 °C and a H_2 pressure of 68 atm within 1 h. The hydrogenation pathway at the strong or Brønsted acid sites favored hydrocracking by forming carbonium ion intermediates that could be hydrogenated by spillover H_2, which was undesirable. On the other hand, the hydrogenation pathway at the weak or Lewis acid sites favored the hydrogenation of aromatic molecules by generating intermediates that could be hydrogenated to produce the saturated hydrogenated product. This was due to the fact that aromatic molecules with π-bonds could act as electron donors for the electron deficient Lewis acid sites. Since the number of weak acid sites increased as the Si/Al ratio decreased, the Rh_1/Al_5-MCF catalyst emerged as the most effective catalyst for the

Published on 13 March 2019. Downloaded by National Synchrotron Radiation Research on 1/9/2020 4:40:19 AM.

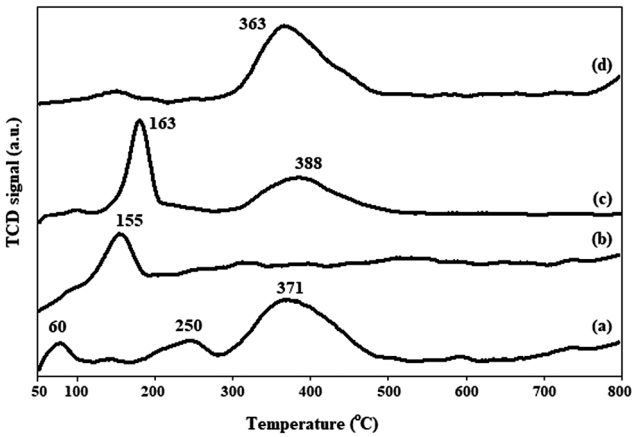

Fig. 9 H_2-TPR thermograms of the synthesized catalysts: (a) Rh_1/MCF, (b) Rh_1/Al_{20}-MCF, (c) Rh_1/Al_{10}-MCF and (d) Rh_1/Al_5-MCF.

Table 4 Results for the surface modification of MCF with Al on catalytic performance

Entry	Catalyst	Si/Al ratio	Conversion (%)
1	Rh_1/Al_{20}-MCF	20	45
2	Rh_1/Al_{10}-MCF	10	62
3	Rh_1/Al_5-MCF	5	100
4	Rh_1/MCF	—	29
5	Rh_1/SBA-15	—	3.5

hydrogenation of DOP to DEHHP. The interaction between Rh and MCF was also believed to be enhanced by Al modification, due to the fact that the Rh nanoparticles formed strong bonds with the surface OH groups of the Al species that were in turn bonded to MCF. The most appropriate interaction between metal and support was observed at a Si/Al ratio of 5. Since the Rh_1/Al_5-MCF catalyst provided the highest conversion of DOP to DEHHP in 1 h of reaction time, it was used for further studies. It must also be noted that no undesirable side products whatsoever were observed for the hydrogenation of DOP using the synthesized Rh_1/Al_5-MCF catalyst, showing that it was 100% selective for the phthalate-free plasticizer DEHHP.

Effect of reaction temperature

The effect of temperature on the hydrogenation of DOP to DEHHP was studied for a temperature range of 40–100 °C at a fixed H_2 pressure of 68 atm for 1 h over the synthesized Rh_1/Al_5-MCF catalyst. As can be read from Fig. 10, only 21% conversion of DOP to DEHHP was achieved at the lowest studied temperature of 40 °C. The conversion was seen to gradually increase with increasing temperature, and 100% conversion was reached at 80 °C. The reactions at temperatures above 80 °C showed no changes in the product distribution and the selectivity of DEHHP was retained. Therefore, 80 °C was chosen as the optimum temperature for this study. This was a 160 °C reduction over the temperature required for the hydrogenation of DOP to DEHHP using supported Ni catalysts, reported in the open literature.[7] This reduction was attributed to the use of a more active metal, Rh, and the modification of the surface properties of the support by incorporating Al.

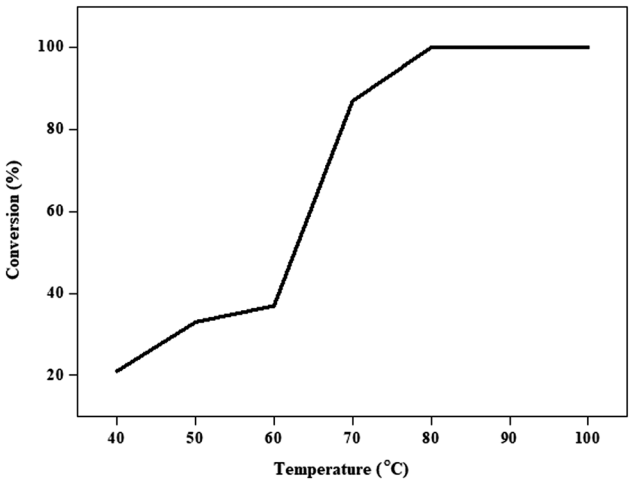

Fig. 10 Effect of reaction temperature on the conversion of DOP to DEHHP.

Effect of H_2 pressure

The influence of H_2 pressure on the hydrogenation of DOP to DEHHP was studied for a pressure range of 34–68 atm at 80 °C for 1 h over the synthesized Rh_1/Al_5-MCF catalyst. It can be seen from Fig. 11 that the conversion of DOP to DEHHP was directly proportional to increasing pressure and increased gradually from 38% at 34 atm H_2 pressure to 100% at 68 atm H_2 pressure. The higher conversion of DOP at increasing H_2 pressures at reaction times as low as 1 h was attributed to the increased availability of H_2 species to undergo H_2 dissociation at active Rh sites and subsequently take part in and speed up the reaction. Sharma *et al.* observed a similar dependence on H_2 pressure for the hydrogenation of benzene to cyclohexane over a Ru-containing hydrotalcite catalyst.[39] The Rh_1/Al_5-MCF catalyst generated more H atoms by increased H_2 spillover, due to the fact that it possessed a high number of active acid sites. Hence, the optimum hydrogen pressure for this study was found to be 68 atm.

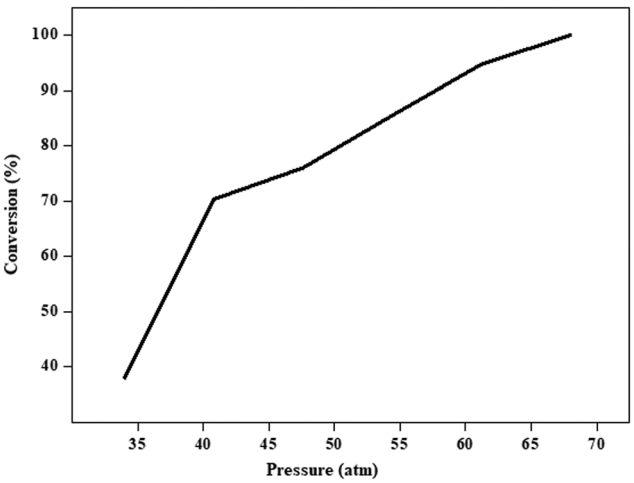

Fig. 11 Effect of H_2 pressure on the conversion of DOP to DEHHP.

 This journal is © The Royal Society of Chemistry and the Centre National de la Recherche Scientifique 2019

Published on 13 March 2019. Downloaded by National Synchrotron Radiation Research on 1/9/2020 4:40:19 AM.

Conclusion

In this work, the effect of the presence of Al in MCF with different Si/Al ratios on the performance of Rh_1/Al-MCF catalysts was systematically studied for the solvent-free hydrogenation of DOP to DEHHP. Al-MCF was synthesized using a post-synthetic method, and Rh was incorporated into the Al-MCF supports through CFD. The physicochemical properties of all the synthesized catalysts were characterized using various analytical techniques. The results demonstrated that MCF retained its meso-structure after incorporation with Al and Rh. Al incorporated onto the framework of MCF contributed to an increase in the total number of acid sites and helped accomplish complete hydrogenation. In addition, the interaction of Rh with the support became stronger with increasing Al doping and reached a maximum at a Si/Al ratio of 5.

100% conversion of DOP to DEHHP with no side products was achieved within 1 h of reaction at a Si/Al ratio of 5, a temperature of 80 °C and a H_2 pressure of 68 atm for the synthesized Rh_1/Al_5-MCF catalyst. This conversion was almost 3.5 times the conversion obtained using the Rh_1/MCF catalyst without any Al modification under the same reaction conditions. Solvent-free hydrogenation under mild reaction conditions with a green catalyst synthesis makes this reaction a candidate for a green and sustainable process.

Conflicts of interest

There are no conflicts to declare.

Acknowledgements

The authors would like to acknowledge the financial support of the Ministry of Science and Technology, ROC, grant number (MOST 106-2622-8-007-017) and the National Tsing Hua University, Taiwan, ROC.

Notes and references

1 S. M. Richardson, S. Bosch, S. Swarts, F. Llados and D. A. Gray, *Toxicological profile for di(2-ethylhexyl) phthalate*, ATSDR and SRC Press, Georgia, NY, 2002.
2 J. Zhang, L. Liu, X. Wang, Q. Huang, M. Tian and H. Shen, *Environ. Sci. Technol.*, 2016, **50**, 5953–5960.
3 Y. J. Ding, C. Diao, L. Ma and P. Lin, *CN Pat.*, 200810224900, 2008.
4 H. Bohnen, T. Klein and K. Bergrath, *US Pat.*, 9051A1, 2003.
5 S. L. Cook, G. Irick and C. S. Moorehouse, *US Pat.*, 5202475A, 2005.
6 S. Liu, C. Xie, S. Yu, F. Liu and Z. Song, *Ind. Eng. Chem. Res.*, 2011, **50**, 2478–2481.
7 J. Zhao, M. Xue, Y. Huang and J. Shen, *Catal. Commun.*, 2011, **16**, 30–34.
8 M. Grass, A. Kaizik, W. Bueschken, A. Tuchlenski, D. Maschmeyer, K. A. Gaudschun and F. Brocksien, *US Pat.*, 7361714B2, 2008.
9 H. Bohnen, T. Klein and K. Bergrath, *US Pat.*, 20030009051Al, 2004.
10 H. K. Chang, C. H. Lee, K. C. Wu and H. Y. Hsu, *US Pat.*, 150614A1, 2013.
11 D. H. Phan-Vu and C. S. Tan, *RSC Adv.*, 2017, **7**, 18178–18188.
12 C. H. Xiang, L. Jinyong and J. S. Timothy, *Environ. Sci. Technol.*, 2018, **52**, 4235–4243.
13 R. Baumgartner and K. McNeill, *Environ. Sci. Technol.*, 2012, **46**, 10199–10205.
14 S. Hu, M. Xue, H. Chen and J. Shen, *Chem. Eng. J.*, 2010, **162**, 371–379.
15 A. C. Gluhoi, P. Marginean and U. Stanescu, *Appl. Catal., A*, 2005, **294**, 208–214.
16 C. H. Yen, H. W. Lin and C. S. Tan, *Catal. Today*, 2011, **174**, 121–126.
17 T. Yasmin and K. Muller, *J. Chromatogr. A*, 2011, **1218**, 6464–6475.
18 D. J. N. Subagyono, M. Marshall, G. P. Knowles and A. L. Chaffee, *Microporous Mesoporous Mater.*, 2014, **186**, 84–93.
19 S. Chen, J. Li, Y. Zhang, Y. Zhao and J. Hong, *Catal. Sci. Technol.*, 2013, **3**, 1063–1068.
20 R. L. Oliveira, T. Nijholt, M. Shakeri, P. E. de Jongh, R. J. M. Klein Gebbink and K. P. de Jong, *Catal. Sci. Technol.*, 2016, **6**, 5124–5133.
21 D. Zhao, J. Feng, Q. Hua, N. Melosh, G. H. Fredrickson, B. F. Chmelka and G. D. Stucky, *Science*, 1998, **279**, 548–552.
22 L. Huang, Z. M. Xing, Y. Kou, L. Y. Shi, X. Q. Liu, Y. Jiang and L. B. Sun, *Ind. Eng. Chem. Res.*, 2018, **57**, 3561–3566.
23 M. X. Gu, Y. Kou, S. C. Qi, M. Q. Shao, M. B. Yue, X. Q. Liu and L. B. Sun, *ACS Sustainable Chem. Eng.*, 2019, **7**, 2837–2843.
24 C. Niklasson and G. Smedler, *Ind. Eng. Chem. Res.*, 1987, **26**, 403–410.
25 S. Song, X. Yang, B. Wang, X. Zhou, A. Duan, K. Chi, Z. Zhao, C. Xu, Z. Chen and J. Li, *Chin. J. Catal.*, 2017, **38**, 1347–1359.
26 P. Kustrowski, L. Chmielarz, R. Dziembaj, P. Cool and E. F. Vansant, *J. Phys. Chem. B*, 2005, **109**, 11552–11558.
27 D. P. Debecker, C. Boissiere, G. Laurent, S. Huet, P. Eliaers, C. Sanchez and R. Backovc, *Chem. Commun.*, 2015, **51**, 14018–14021.
28 W. Yu, Y. P. Hsu and C. S. Tan, *Appl. Catal., B*, 2016, **196**, 185–192.
29 C. H. Yen, H. W. Lin, T. D. Phan and C. S. Tan, *J. Nanosci. Nanotechnol.*, 2011, **11**, 2465–2469.
30 H. W. Lin, C. H. Yen, Y. P. Hsu and C. S. Tan, *RSC Adv.*, 2013, **3**, 17222–17227.
31 J. Lim, S. S. Lee and J. Y. Ying, *Chem. Commun.*, 2010, **46**, 806–808.
32 J. C. Park, J. I. Kwon, S. W. Kang, D. H. Chun, H. Jung, H. T. Leea and J. I. Yang, *New J. Chem.*, 2016, **40**, 9586–9592.
33 Y. Miao, G. Lu, X. Liu, Y. Guo, Y. Wang and Y. Guo, *Microporous Mesoporous Mater.*, 2009, **122**, 55–60.
34 A. R. Huirache, B. Pawelec, E. R. Munoz, R. Nava, J. Espino and J. L. G. Fierro, *Appl. Catal., B*, 2009, **92**, 168–184.
35 L. Zhu, X. Q. Liu, H. L. Jiang and L. B. Sun, *Chem. Rev.*, 2017, **117**, 8129–8176.
36 H. J. Chae, T. W. Kim, Y. K. Moon, H. K. Kim, K. E. Jeong, C. U. Kim and S. Y. Jeong, *Appl. Catal., B*, 2014, **150**, 596–604.
37 M. Piumetti, M. Hussain, D. Fino and N. Russo, *Appl. Catal., B*, 2015, **165**, 158–168.
38 S. Bhattacharjee, W. Y. Lu and C. S. Tan, *Fuel*, 2019, **243**, 210–220.
39 S. K. Sharma, K. B. Sidhpuria and R. V. Jasra, *J. Mol. Catal. A: Chem.*, 2011, **335**, 65–70.